CHEMISTRY
A EUROPEAN JOURNAL

DOI: 10.1002/chem.200500972

A Variety of Spin-Crossover Behaviors Depending on the Counter Anion: Two-Dimensional Complexes Constructed by NH···Cl^- Hydrogen Bonds, $[Fe^{II}H_3L^{Me}]Cl{\cdot}X$ ($X = PF_6^-$, AsF_6^-, SbF_6^-, $CF_3SO_3^-$; H_3L^{Me} = Tris[2-{[(2-methylimidazol-4-yl)methylidene]amino}ethyl]amine)

Masahiro Yamada,[a] Hiroaki Hagiwara,[a] Haruna Torigoe,[a] Naohide Matsumoto,*[a] Masaaki Kojima,[b] Françoise Dahan,[c] Jean-Pierre Tuchagues,[c] Nazzareno Re,[d] and Seiichiro Iijima[e]

Abstract: A family of spin-crossover (SC) complexes, $[Fe^{II}H_3L^{Me}]Cl{\cdot}X$ (X^- = PF_6^-, AsF_6^-, SbF_6^-, $CF_3SO_3^-$), **1**–**4**, has been synthesized, in which H_3L^{Me} denotes the hexadentate N_6 tripod-like ligand tris[2-{[(2-methylimidazol-4-yl)-methylidene]amino}ethyl]amine, containing three imidazole groups, with a view to establishing the effect of the counter anion on the SC behavior. These complexes have been found to crystallize in the same monoclinic crystal system with similar cell dimensions. The general crystal structure consists of a two-dimensional (2D) extended network constructed by NH···Cl^- hydrogen bonds between Cl^- and the imidazole NH groups of three neighboring $[Fe^{II}H_3L^{Me}]^{2+}$ ions, while the anion X exists as an isolated counter anion and occupies the space between the 2D sheets. Magnetic susceptibilities and Mössbauer spectra have revealed a variety of SC behaviors depending on the counter anion, including a one-step HS $\rightleftarrows$ (HS + LS)/2 (**1**, X = PF_6^-), a two-step HS $\rightleftarrows$ (HS + LS)/2 $\rightleftarrows$ LS with a slow thermal relaxation (**2**, X = AsF_6^-), a gradual one-step HS $\rightleftarrows$ LS (**3**, X = SbF_6^-), and a steep one-step HS $\rightleftarrows$ LS with hysteresis (**4**, X = $CF_3SO_3^-$). The complexes assume the space group $P2_1/n$ in the HS state, $P2_1$ in the HS + LS state, and $P2_1/n$ in the LS state. The Fe–N bond lengths and the N-Fe-N bond angles are indicative of the HS, HS + LS, and LS states. The molecular volumes, *V*, of the counter anions have been evaluated by quantum-chemical calculations as follows: 53.4 Å^3 (BF_4^-), 54.4 Å^3 (ClO_4^-), 73.0 Å^3 (PF_6^-), 78.5 Å^3 (AsF_6^-), 88.7 Å^3 (SbF_6^-), and 86.9 Å^3 ($CF_3SO_3^-$). The size and shape of the counter anion affects the flexible 2D network structure constructed by the hydrogen bonds, leading to modifications of the SC behavior. These estimated relative sizes of the counter anions correlate well with the observed SC behaviors.

Keywords: hydrogen bonds · iron · magnetic properties · Mössbauer spectroscopy · spin crossover

[a] M. Yamada, H. Hagiwara, H. Torigoe, Prof. Dr. N. Matsumoto
Department of Chemistry, Faculty of Science
Kumamoto University
Kurokami 2–39–1, Kumamoto 860–8555 (Japan)
Fax: (+81) 96-342-3390
E-mail: naohide@aster.sci.kumamoto-u.ac.jp

[b] Prof. Dr. M. Kojima
Department of Chemistry, Faculty of Science
Okayama University
Tsushima-naka 3–1–1, Okayama 700–8530 (Japan)

[c] Dr. F. Dahan, Prof. Dr. J.-P. Tuchagues
Laboratoire de Chimie de Coordination du CNRS, UP 8241
205 Route de Narbonne, 31077 Toulouse cedex (France)

[d] Prof. Dr. N. Re
Facolta di Farmacia
Università degli Studi "G. D'Annunzio"
66100 Chieti (Italy)

[e] Dr. S. Iijima
National Institute of Advanced Industrial Science and Technology,
Tsukuba 305–8566 (Japan)

Supporting information for this article is available on the WWW under http://www.chemeurj.org/ or from the author.

Introduction

Spin-crossover (SC) is a representative example of molecular bistability, in which the high-spin (HS) and low-spin (LS) states are interconvertible by physical perturbations such as a change in temperature, pressure, an external magnetic field, or irradiation with light.[1,2] While SC behavior is essentially a phenomenon of individual molecules, the interaction between the SC sites is an important factor governing the SC properties such as the steepness and multistep nature of the spin transition, hysteresis, and the LIESST (light-induced excited spin state trapping) effect, which are important properties with regard to applications in information storage, molecular switches, and visual displays.[3] The synthesis of SC compounds exhibiting interactions between the SC sites is of current interest. For example, in the current decade, polymeric SC compounds with bridging ligands[4] and mononuclear SC compounds exhibiting inter-

molecular interactions such as hydrogen bonding and π–π stacking[5] have been extensively investigated, and they have been found to show interesting SC behavior. It is also known that the presence of solvent molecules in the crystal lattice and the nature of the counter anion significantly affect the SC behavior, although such species do not directly interact with the SC site.[6] This highlights the need for a more systematic investigation of such subfactors, as well as for a rational explanation of the complicated results.

We have investigated metal complexes containing imidazole groups.[7] Of these, iron complexes with tripod ligands containing three imidazole groups, H_3L^R (R = H, Me, Ph), H_3L^R = tris[2-{[(2-R-imidazoyl-4-yl)methylidene]amino}-ethyl]amine, have been found to constitute a new family of SC complexes.[6] These systems comprise $[Fe^{II}H_3L^R]X_2$, $[Fe^{III}H_3L^R]X_3$, $[Fe^{III}L^R]$, $[Fe^{II}H_3L^R][Fe^{II}L^R]X$, and $[Fe^{II}H_3L^R][Fe^{III}L^R]X_2$ complexes, where X denotes a mononegative anion such as ClO_4^- or PF_6^-. In particular, complexes of the type $[Fe^{II}H_3L^R][Fe^{II}L^R]X$ and $[Fe^{II}H_3L^R]$-$[Fe^{III}L^R]X_2$, in which two component Fe sites, $[Fe^{II}H_3L^R]^{2+}$ and $[Fe^{II}L^R]^-$ or $[Fe^{III}L^R]^0$, are connected through an imidazole–imidazolate hydrogen bond to produce a two-dimensional (2D) extended network structure, have been found to exhibit steep and multistep SC behavior.[6] We have also identified another new type of 2D SC complex with the chemical formula $[Fe^{II}H_3L^{Me}]Cl{\cdot}I_3$.[8] This compound shows a steep spin transition, and the crystal structure consists of a new type of 2D extended network constructed by NH···Cl^- hydrogen bonds. Since we have already shown that the counter anion in $[Fe^{II}H_3L^{Me}][Fe^{II}L^{Me}]X$ significantly affects the SC properties,[6] it was anticipated that the counter anion in $[Fe^{II}H_3L^{Me}]Cl{\cdot}X$ may have a similar influence. Variation of X would then allow us to address the issue of how the counter anion modifies the SC behavior of the 2D complex through intra- and interlayer elastic interactions. Towards this objective, a series of complexes with the general formula $[Fe^{II}H_3L^{Me}]Cl{\cdot}X$ (X^- = PF_6^-, AsF_6^-, SbF_6^-, or $CF_3SO_3^-$) has been prepared. Depending on the counter anion, this series of complexes has been found to exhibit a variety of SC behaviors, including a one-step (HS ⇄ (HS + LS)/2), a two-step (HS ⇄ (HS + LS)/2 ⇄ LS) with slow thermal relaxation, a gradual one-step (HS ⇄ LS), and a steep one-step (HS ⇄ LS) transition with hysteresis. We now report the 2D structure constructed by NH···Cl^- hydrogen bonds between the imidazole groups of the complex cation and Cl^- ions, the detailed crystal structures of the HS, (HS + LS)/2, and LS states, and a variety of SC behaviors as revealed by the temperature dependences of the magnetic susceptibilities and the Mössbauer spectra.

Results and Discussion

Synthesis and characterization of $[Fe^{II}H_3L^{Me}]Cl{\cdot}X$ (X^- = PF_6^-, AsF_6^-, SbF_6^-, $CF_3SO_3^-$): Fe^{II} complexes with the formulas $[Fe^{II}H_3L^{Me}]X_2$ (X^- = ClO_4^-, BF_4^-) and $[Fe^{II}H_3L^{Me}]Cl{\cdot}X$ (X^- = AsF_6^-, SbF_6^-, $CF_3SO_3^-$) were easily obtained as orange or dark-orange crystals by mixing the neutral form of the tripodal ligand H_3L^{Me} (H_3L^{Me} = tris[2-{[(2-methylimidazol-4-yl)methylidene]amino}ethyl]amine), $Fe^{II}Cl_2{\cdot}4H_2O$, and NaX in a 1:1:2 molar ratio in methanol, without protection from air, as detailed in the Experimental Section. A combination of the Fe^{II} complex cation with the neutral ligand, $[Fe^{II}H_3L^{Me}]^{2+}$, and a rather small counter anion, such as ClO_4^- or BF_4^-, crystallized with the chemical formula $[Fe^{II}H_3L^{Me}]X_2$, whereas a combination of this complex cation with a larger counter anion, such as AsF_6^-, SbF_6^-, or $CF_3SO_3^-$, crystallized with the chemical formula $[Fe^{II}H_3L^{Me}]Cl{\cdot}X$. The PF_6^- salt was found to crystallize from MeOH with the formula $[Fe^{II}H_3L^{Me}]Cl{\cdot}PF_6{\cdot}MeOH$, a high-spin complex over the temperature range 5–300 K that showed distinctly different magnetic properties from those of the compound without methanol. The compound without the solvent of crystallization, $[Fe^{II}H_3L^{Me}]Cl{\cdot}PF_6$ (**1**), can be obtained by performing the reaction in H_2O/CH_3CN. It should be noted that anaerobic conditions are not always necessary for the syntheses of the present Fe^{II} complexes. X-ray crystal structures at selected temperatures were determined for all of the complexes. The crystallographic data are summarized in Table 1. They indicate that all of the complexes crystallized in the same monoclinic space group with very similar crystal dimensions. All of the IR spectra for the series of complexes with the neutral ligand showed a characteristic sharp single band at around 1640 cm^{-1} at ambient temperature due to the C=N stretching vibration of the Schiff-base ligand, which can be assigned to the HS Fe^{II} state.[6,9]

SC properties and structures of $[Fe^{II}H_3L^{Me}]Cl{\cdot}X$ (X^- = PF_6^-, AsF_6^-, SbF_6^-, $CF_3SO_3^-$)

General: The SC behavior of the complexes was investigated by measuring their temperature-dependent magnetic susceptibilities, as well as by Mössbauer spectroscopy and X-ray analyses. The general procedures outlined below were used, unless otherwise noted. The magnetic susceptibilities were measured in the 5–300 K temperature range, at a sweep rate of 1 K min^{-1}, in an applied magnetic field of 1 T. The sample was quickly cooled from room temperature to 5 K, and the magnetic susceptibility was measured in the warming mode from 5 to 300 K as a first run and then measured in the cooling mode from 300 to 5 K as a second run. Mössbauer spectra were recorded in the 4.2–298 K range. The sample was initially cooled from room temperature to 4.2 K within 3 min and Mössbauer spectra were then measured in the warming and cooling modes. Crystal structures were determined by single-crystal X-ray diffraction analyses at the appropriate temperatures to confirm the spin states. Table 1 summarizes the crystallographic data for all of the complexes at the selected temperatures. These complexes not only crystallized in the same monoclinic crystal system with similar cell dimensions, but also assumed the same space groups, that is, $P2_1/n$ in the HS state, $P2_1$ in the HS + LS state, and $P2_1/n$ in the LS state. All complexes in the HS

Table 1. Crystallographic data for complexes **1**–**4**.

	1			**2**			**3**	**4**
	296 K	93 K	180 K	110 K	90 K	180 K	90 K	296 K
formula	$C_{21}H_{30}ClF_6FeN_{10}P$	$C_{21}H_{30}ClF_6FeN_{10}P$	$C_{21}H_{30}AsClF_6FeN_{10}$	$C_{21}H_{30}AsClF_6FeN_{10}$	$C_{21}H_{30}AsClF_6FeN_{10}$	$C_{21}H_{30}ClF_6FeN_{10}Sb$	$C_{21}H_{30}ClF_6FeN_{10}Sb$	$C_{22}H_{30}ClF_3FeN_{10}O_3S$
Fw	658.80	658.80	702.75	702.75	702.75	749.60	749.60	662.90
crystal system	monoclinic	monoclinic	monoclinic	monoclinic	monoclinic	monoclinic	monoclinic	monoclinic
space group	$P2_1/n$ (no. 14)	$P2_1$ (no. 4)	$P2_1/n$ (no. 14)	$P2_1$ (no. 4)	$P2_1/n$ (no. 14)	$P2_1/n$ (no. 14)	$P2_1/n$ (no. 14)	$P2_1/n$ (no. 14)
a [Å]	17.501(5)	17.212(5)	17.450(5)	17.230(6)	17.089(5)	17.5367(14)	17.2127(14)	18.055(4)
b [Å]	13.212(4)	12.680(4)	13.096(3)	12.796(3)	12.522(6)	13.2154(10)	12.7252(11)	12.636(4)
c [Å]	13.105(4)	13.109(6)	13.068(3)	13.090(3)	13.104(7)	13.1112(11)	13.0765(11)	13.589(4)
β [°]	96.51(1)	95.57(1)	96.53(1)	95.44(1)	94.88(2)	95.817(7)	94.727(7)	98.62(1)
V [Å^3]	3010(1)	2847(1)	2967(1)	2873(1)	2794(2)	3022.9(4)	2854.5(4)	3065(1)
Z	4	4	4	4	4	4	4	4
F(000)	1352	1352	1424	1424	1424	1496	1496	1368
λ [Å]	0.71075	0.71075	0.71075	0.71075	0.71075	0.71073	0.71073	0.71073
T [K]	296 ± 2	93 ± 2	180 ± 2	110 ± 2	90 ± 2	180 ± 2	90 ± 2	296 ± 2
ρ_{calcd} [Mg m^{-3}]	1.453	1.536	1.537	1.625	1.670	1.647	1.744	1.436
$\mu(Mo_{K\alpha})$ [mm^{-1}]	7.09	7.50	17.73	18.31	18.83	15.27	16.17	7.07
θ range [° min–max]	3.1–27.5	3.1–27.5	3.1–27.5	3.1–27.6	3.1–27.5	2.13–26.04	3.23–32.37	3.0–27.5
no. of data collected	29321	26630	29167	28156	25898	30088	27838	30324
no. of unique data	6872	12777	6745	12867	6365	9965	9378	7022
R(int)	0.023	0.027	0.047	0.048	0.216	0.034	0.043	0.022
no. of variable parameters	391	782	391	782	391	406	406	400
no. of obsd. refl.[a]	4695	11438	4199	9417	1557	5660	6333	5024
R[b] obsd., all	0.061, 0.077	0.044, 0.049	0.061, 0.090	0.052, 0.072	0.120, 0.219	0.041, 0.077	0.042, 0.063	0.045, 0.058
Rw[c] obsd., all	0.192	0.130	0.180	0.136	0.289	0.092, 0.105	0.096, 0.107	0.144
S	1.001	0.999	0.999	0.998	0.850	0.879	0.956	0.992
$(\Delta/\sigma)_{max}$	0.000	0.000	0.000	0.000	0.007	0.001	0.001	0.000
$(\Delta/\rho)_{max,min}$ [e Å^{-3}]	1.13, −0.61	1.76, −1.17	1.75, −1.89	2.14, −1.91	3.22, −2.93	1.09, −0.63	0.857, −0.722	1.98, −0.63

[a] Data with $F_o > 4\sigma(F_o)$. [b] $R = \Sigma||F_o|-|F_c||/\Sigma|F_o|$. [c] $Rw = [\Sigma w(|F_o^2|-|F_c^2|)^2/\Sigma w|F_o^2|^2]^{1/2}$.

and LS states assume a similar 2D extended structure, and so, except for the anions, the same atom numbering scheme applies throughout. Complexes **1** and **2** in the HS + LS state assume similar 2D structures and, except for the anions, the same atom numbering scheme applies.

$[Fe^{II}H_3L^{Me}]Cl{\cdot}PF_6$ (1): Figure 1 shows $\chi_M T$ versus T plots for the warming and cooling modes, where $\chi_M T$ is the molar magnetic susceptibility and T is the absolute temperature. The magnetic behaviors in the warming and cooling modes are almost the same and show an SC of the HS ⇄ (HS + LS)/2 type. In the 300–150 K region, the $\chi_M T$ value is nearly constant at about 3.5 cm^3 K mol^{-1}, as expected for an HS Fe^{II} species ($S = 2$). Upon further cooling of the sample in the 150–100 K region, the $\chi_M T$ value abruptly decreases at around 130 K, and then reaches a plateau value of about 1.8 cm^3 K mol^{-1} below 100 K. This $\chi_M T$ value of 1.8 cm^3 K mol^{-1} is approximately half of the 3.5 cm^3 K mol^{-1} observed in the HS temperature region, indicating that one of two Fe^{II} sites converts to the LS state, while the other remains in the HS state (HS ⇄ (HS + LS)/2); a value of $T_{1/2}$ = 122 K for the HS ⇄ (HS + LS)/2 transition was evaluated from the first derivative of $\chi_M T$.

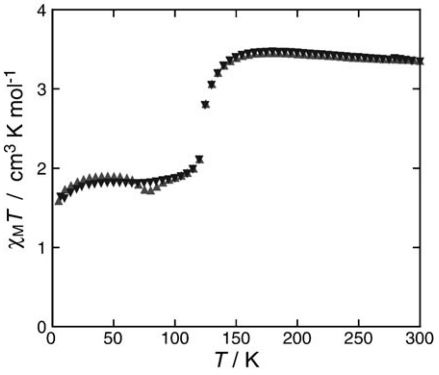

Figure 1. Magnetic behavior of $[Fe^{II}H_3L^{Me}]Cl{\cdot}PF_6$ (**1**) in the form of $\chi_M T$ versus T plots in the warming and cooling modes. The sample was quickly cooled from 300 K to 5 K and $\chi_M T$ was first measured in the course of warming from 5 to 300 K at a sweep rate of 1 K min^{-1} (▲). Values were then measured in the course of cooling from 300 to 5 K at a sweep rate of 1 K min^{-1} (▼).

Selected Mössbauer spectra in the warming mode are shown in Figure 2, which serve to corroborate the HS ⇄ (HS + LS)/2 SC behavior. Table 2 lists the Mössbauer parameters at each selected temperature in the warming and cooling modes. The Mössbauer spectra in the warming and cooling modes are nearly the same, showing that there is no frozen-in effect. In the temperature region 4.2–120 K, each spectrum consists of two doublets attributable to the HS Fe^{II} species (for example, at 4.2 K, isomer shift δ = 1.12 mm s^{-1}, quadrupole splitting ΔE_Q = 2.18 mm s^{-1}) and the LS Fe^{II} species (at 4.2 K, δ = 0.47 mm s^{-1} and ΔE_Q = 0.22 mm s^{-1}),

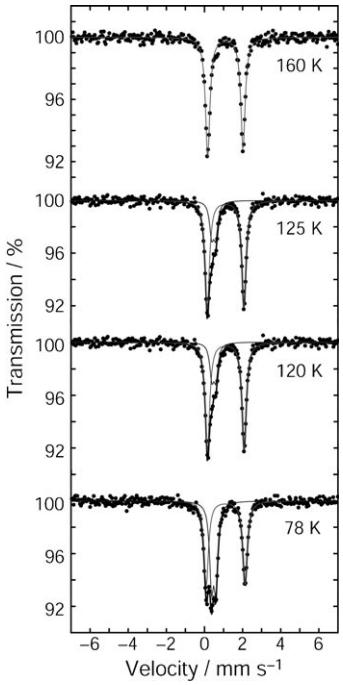

Figure 2. Selected ^{57}Fe Mössbauer spectra of $[Fe^{II}H_3L^{Me}]Cl{\cdot}PF_6$ (**1**) recorded at 78, 120, 125, and 160 K upon warming the sample from 78 K.

Table 2. Mössbauer data for $[Fe^{II}H_3L^{Me}]Cl{\cdot}PF_6$ (**1**).

A. On heating after rapid cooling to 4.2 K				
T [K]	δ[a] [mm s^{-1}]	ΔE_Q [mm s^{-1}]	Γ[b] [mm s^{-1}]	Area ratio [%]
298	0.98	1.76	0.27	100
200	1.07	1.83	0.27	100
160	1.09	1.85	0.28	100
140	1.10	1.88	0.27	90
	0.45	0.23	0.25	10
130	1.11	1.90	0.27	83
	0.48	0.22	0.28	17
125	1.11	1.92	0.27	77
	0.48	0.21	0.26	23
120	1.11	2.03	0.28	55
	0.48	0.22	0.25	45
110	1.12	2.08	0.28	52
	0.48	0.22	0.25	48
78	1.10	2.16	0.27	50
	0.47	0.23	0.26	50
4.2	1.12	2.18	0.26	52
	0.47	0.22	0.26	48
B. On slow cooling from room temperature				
T [K]	δ[a] [mm s^{-1}]	ΔE_Q [mm s^{-1}]	Γ[b] [mm s^{-1}]	Area ratio [%]
78	1.12	2.15	0.27	51
	0.49	0.22	0.26	49
4.2	1.13	2.17	0.27	53
	0.49	0.22	0.25	47

[a] Isomer shift data are reported with respect to iron foil. [b] Full width at half-height.

in an area ratio of 1:1. Upon increasing the sample temperature from 120 to 160 K, the relative intensity of the doublet due to the HS Fe^{II} species increases, while the doublet due to the LS Fe^{II} species decreases and ultimately disappears. At 298, 200, and 160 K, each spectrum consists only of a doublet attributable to the HS Fe^{II} species. A deconvolution analysis was performed to determine the HS versus total Fe^{II} molar fraction, n_{HS}, and the results are presented in Table 2 and Figure 3. The Mössbauer results demonstrate that 50% of the Fe^{II} species is converted from the HS to the LS state, which is consistent with the magnetic susceptibility result.

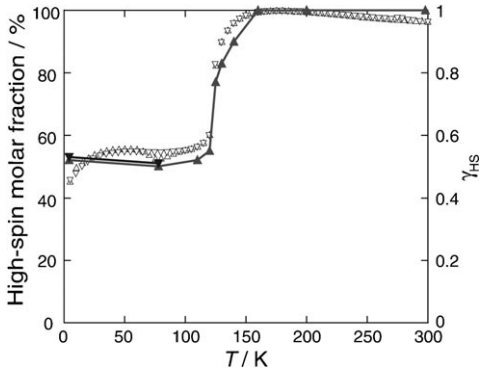

Figure 3. Molar fraction of HS versus total Fe^{II}, n_{HS}, for $[Fe^{II}H_3L^{Me}]Cl{\cdot}PF_6$ (**1**) in the warming (▲) and cooling modes (▼) obtained by deconvolution analysis of the Mössbauer spectra, together with n_{HS} obtained from the magnetic susceptibility measurements. The n_{HS} value from the magnetic susceptibility measurements was calculated using the equation $(\chi_M T)_{obs} = n_{HS}(\chi_M T)_{HS} + (1 - n_{HS})(\chi_M T)_{LS}$, with $(\chi_M T)_{HS} = 3.5\,cm^3\,K\,mol^{-1}$ and $(\chi_M T)_{LS} = 0.0\,cm^3\,K\,mol^{-1}$ as the limiting values.

Since the magnetic susceptibility and Mössbauer spectral measurements demonstrated a one-step spin-crossover between the HS and (HS+LS)/2 states at around 130 K, crystal structures were determined at 296 and 93 K to confirm these two spin states. The unit cell parameters at 296 K are similar to those at 93 K, but the cell volume is reduced by 5.4% upon the spin transition. The space group $P2_1/n$ at 296 K becomes $P2_1$ at 93 K and consequently the number of unique molecules changes from one at 296 K to two at 93 K. Figure 4 and Figure 5 show ORTEP drawings of the unique molecules in the HS and (HS + LS)/2 states, respectively, together with the atom-numbering schemes adopted. Table 3 shows selected bond lengths and hydrogen-bond lengths.

The crystal structures at both temperatures reveal similar 2D networks, in which chloride ions serve as connectors through forming hydrogen bonds to the imidazole NH groups of three neighboring cations $[Fe^{II}H_3L^{Me}]^{2+}$ (see Figure 6a). Figure 6b shows the 2D network structure at 296 K, in which the hydrogen-bond lengths are Cl···N4* = 3.095(3), Cl···N(7)** = 3.065(3), and Cl···N(10) = 3.105(4) Å. It should be noted that all three imidazole NH groups of the $[Fe^{II}H_3L^{Me}]^{2+}$ ion are involved in the construction of the 2D layer structure. The geometry of the ClN_3 unit defined by the Cl^- ion and three hydrogen-bonded imidazole nitrogen atoms is not planar as the four paired electrons of the Cl^- ion are oriented in a tetrahedral geometry. The PF_6^- ion exists as an isolated counter anion. As shown in Figure 6c, each 2D layer assumes a thickness correspond-

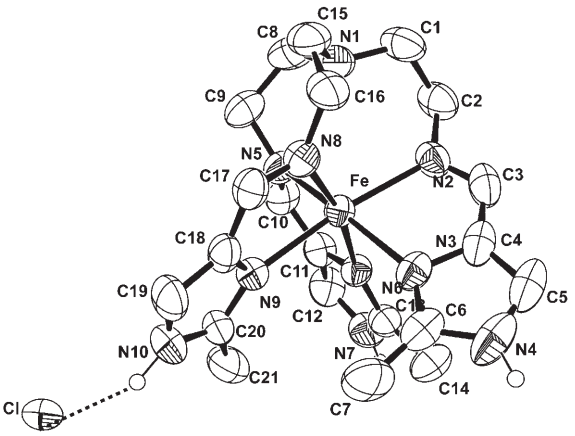

Figure 4. ORTEP drawing of $[Fe^{II}H_3L^{Me}]Cl{\cdot}PF_6$ (**1**) at 296 K (HS state) showing the atom numbering scheme. Since all of the complexes **1**–**4** assume similar cell dimensions and the same space group, $P2_1/n$, in the HS and LS states, the same atom-numbering scheme applies throughout, except for the anions.

Table 3. Relevant coordination bond lengths [Å], angles [°], and hydrogen-bond lengths [Å] for $[Fe^{II}H_3L^{Me}]Cl{\cdot}PF_6$ (**1**) at 296 and 93 K.

	296 K		93 K
Fe1–N2	2.180(3)		2.177(3)
Fe1–N3	2.232(3)		2.214(3)
Fe1–N5	2.192(3)		2.178(3)
Fe1–N6	2.208(3)		2.198(3)
Fe1–N8	2.174(3)		2.164(3)
Fe1–N9	2.221(3)		2.216(3)
Fe2–N12			1.978(3)
Fe2–N13			2.002(3)
Fe2–N15			1.996(3)
Fe2–N16			1.989(3)
Fe2–N18			1.992(3)
Fe2–N19			1.987(3)
hydrogen bonds			
	296 K		93 K
Cl1···N4[a]	3.095(3)	Cl1···N14[a]	3.096(3)
Cl1···N7[b]	3.065(3)	Cl1···N7[b]	3.057(3)
Cl1···N10	3.105(4)	Cl1···N10	3.120(3)
		Cl2···N4[a]	3.092(3)
		Cl2···N17[b]	3.054(3)
		Cl2···N20	3.110(3)

Symmetry operations: [a] $-x, -y, 1-z$; [b] $-x, {}^1/_2+y, {}^3/_2-z$.

ing to two molecular units of the complex, and the 2D layers are separated by a layer of PF_6^- ions. The $[Fe^{II}H_3L^{Me}]^{2+}$ ion is a chiral species with either a Δ (clockwise) or Λ (anticlockwise) configuration due to the screw coordination arrangement of the achiral tripod ligand around the Fe^{II} ion. Within a 2D layer, the Δ and Λ enantiomers are connected by hydrogen bonds in an alternating array, thus making it a racemic rather than homochiral layer. It should be noted that this is in contrast to the 2D layer of $[Fe^{II}H_3L^{Me}][Fe^{II}L^{Me}]X$, constructed through imidazole–imidazolate hydrogen bonds, which is a homochiral layer.[6,7]

At 93 K, the chiral space group $P2_1$ is adopted and the crystallographically unique unit consists of two independent Fe^{II} sites, Fe1 and Fe2. In Figure 5, these can be seen to have different chiralities. Figure 7 shows the 2D structure at 93 K, in which the HS Fe1 and LS Fe2 species are highlighted in red and green, respectively. Two crystallographically unique $[Fe^{II}H_3L^{Me}]^{2+}$ ions represent chiral species with different Δ (clockwise) and Λ (anticlockwise) configurations. Within a 2D layer, the Δ and Λ enantiomers are arranged in an alternating array. As shown in Figure 7, the HS Fe1 sites with the Δ configuration are arranged along the *c*-axis to give a layer structure, interspersed with layers of LS Fe2 sites with the Λ configuration. The spin conversion from the HS to the (HS+LS)/2 state, in other words a stable HS+LS state, can be rationalized in terms of this striped layer structure with different chiralities.

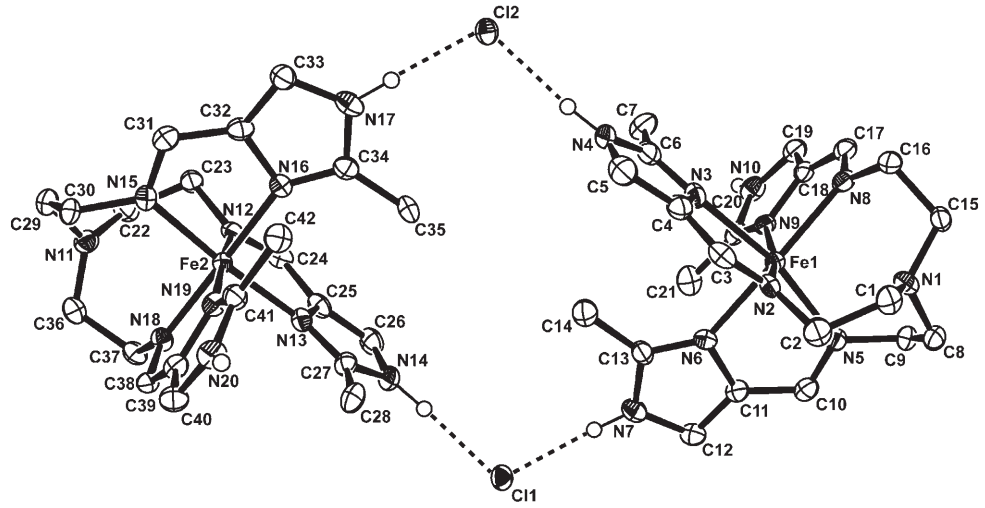

Figure 5. ORTEP drawing of $[Fe^{II}H_3L^{Me}]Cl{\cdot}PF_6$ (**1**) at 93 K ((HS + LS)/2 state) showing the atom-numbering scheme. Complexes **1** and **2** in the HS + LS state assume a similar 2D structure and so, except for the anions, the same atom-numbering scheme applies.

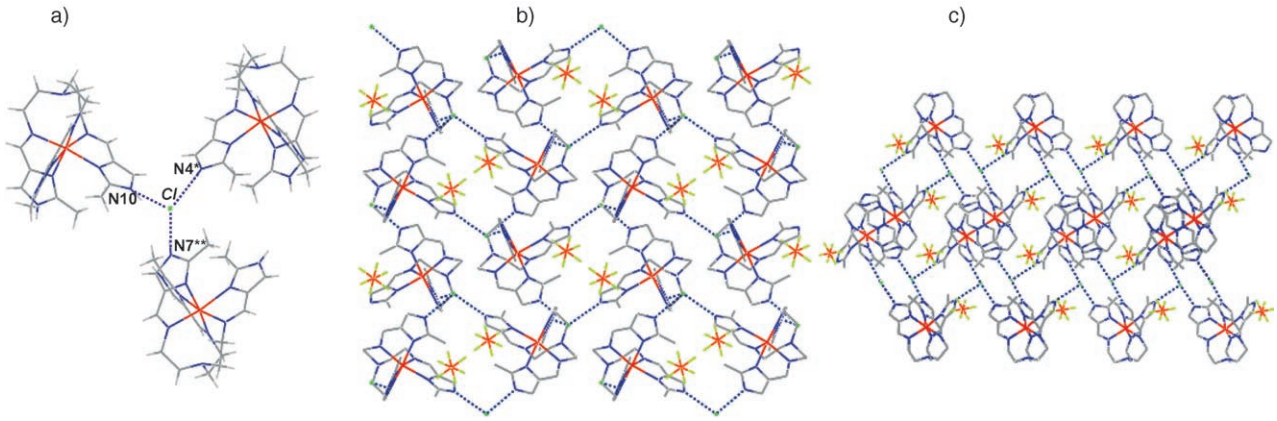

Figure 6. Molecular structure of $[Fe^{II}H_3L^{Me}]Cl{\cdot}PF_6$ (**1**) at 296 K. a) One Cl^- ion is hydrogen-bonded to three imidazole NH groups of three adjacent cationic complexes $[Fe^{II}H_3L^{Me}]^{2+}$. b) Top view of a 2D layer. The $[Fe^{II}H_3L^{Me}]^{2+}$ ions and Cl^- anions are hydrogen-bonded to form a 2D layered structure. The network of the 2D sheet consists of fused dinuclear and tetranuclear cyclic structures made up of two and four $[Fe^{II}H_3L^{Me}]^{2+}$ units, respectively, connected by Cl^--mediated hydrogen bonds. c) Side view showing the stacking of the 2D layers. All of the complexes **1**–**4** in the HS and LS states assume a similar 2D extended structure.

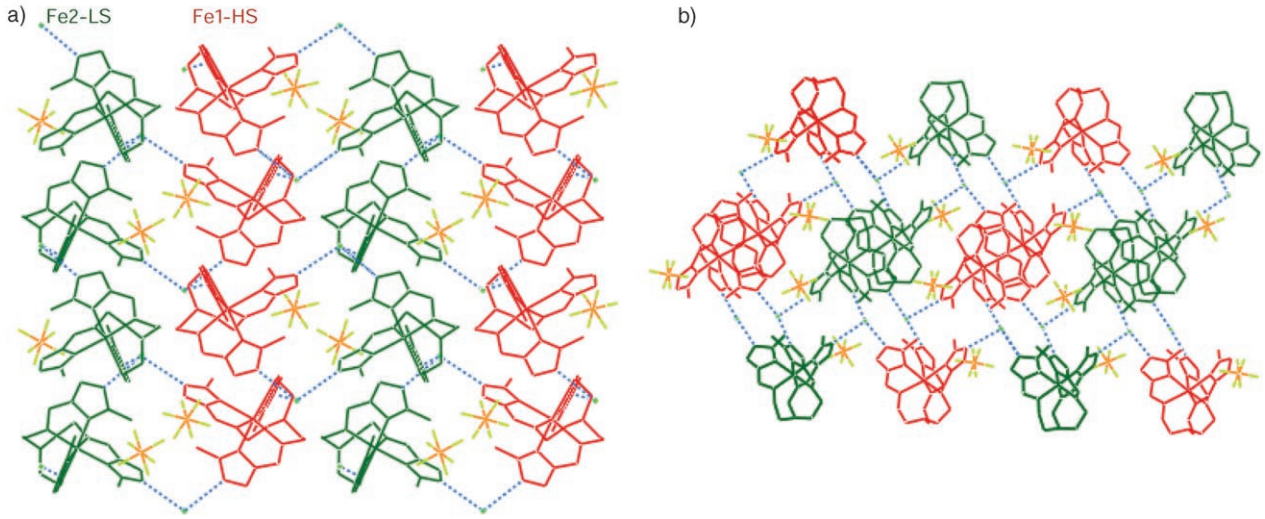

Figure 7. X-ray structure of $[Fe^{II}H_3L^{Me}]Cl{\cdot}PF_6$ (**1**) at 93 K in the HS + LS state. a) Projection on the *ab* plane showing a 2D sheet in which the HS (red) and LS (green) $[Fe^{II}H_3L^{Me}]^{2+}$ components of different chiralities are linked together through the Cl^- ion by hydrogen bonds. b) Side view of a puckered sheet looking along the *b* axis. In this 2D supramolecular structure, the capped tripod-like HS and LS $[Fe^{II}H_3L^{Me}]^{2+}$ components are arranged in alternating up and down orientations. The HS Fe1 sites with the Δ configuration extend along the *c* axis to form a layer structure, interspersed with layers of LS Fe2 sites with the Λ configuration. Complexes **1** and **2** in the HS + LS state assume a similar 2D structure.

The Fe^{II} ion assumes an octahedral coordination environment made up of the six N donor atoms of three Fe–N (imine) bonds and three Fe–N (imidazole) bonds. On the basis of the Fe–N bond lengths and N-Fe-N bond angles, the spin state can be inferred. At 296 K (Figure 4), the Fe–N bond lengths (2.174(4)–2.232(4) Å) are typical of what one would expect for an HS Fe^{II} complex with six similar N donor atoms. At 93 K (Figure 5), the Fe1–N bond lengths (2.164(3)–2.216(3) Å) are characteristic of a high-spin Fe^{II} complex, while the Fe2–N bond lengths (1.978(3)–2.00(3) Å) are characteristic of a low-spin Fe^{II} complex. The difference in the average Fe–N bond lengths at Fe1 and Fe2 is 0.201 Å, which is comparable to the HS-LS difference of about 0.2 Å reported for Fe^{II} SC complexes with the same N_6 donors such as $[Fe^{II}H_3L^{Me}][Fe^{II}L^{Me}]PF_6$.[6c] The N-Fe-N bond angles also indicate that Fe1 assumes the HS state and Fe2 the LS state, since the angle at Fe2 is closer to that of a regular octahedron compared to that at Fe1 (for example, N2-Fe1-N3 = 76.1(1)° and N12-Fe2-N13 = 82.2(1)° at 93 K).

SC properties and structure of $[Fe^{II}H_3L^{Me}]Cl{\cdot}AsF_6$ (2): Figure 8 shows $\chi_M T$ versus T plots for **2**, demonstrating a two-step SC of the type HS ⇄ (HS + LS)/2 ⇄ LS. Considering the first set of measurements, the $\chi_M T$ value of 1.3 $cm^3 K mol^{-1}$ at 5 K after rapid cooling is substantially smaller than that of the HS ($S = 2$) Fe^{II} state and slightly smaller than that for one half of the expected HS ($S = 2$)

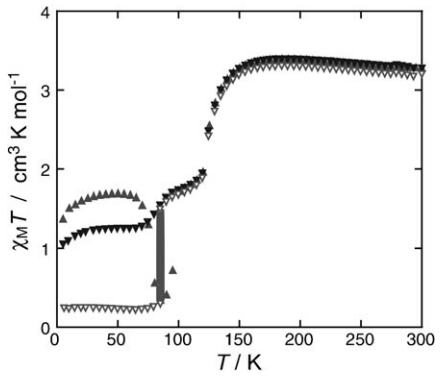

Figure 8. Magnetic behavior of $[Fe^{II}H_3L^{Me}]Cl{\cdot}AsF_6$ (**2**) in the form of $\chi_M T$ versus T plots in the warming and cooling modes. The sample was quickly cooled from 300 to 5 K within a few seconds and $\chi_M T$ was first measured in the course of warming from 5 to 300 K at a sweep rate of 1 K min^{-1} (▲). It was then measured in the course of cooling from 300 to 5 K at a sweep rate of 1 K min^{-1} (▼). When the sample was maintained at 85 K for 750 min after cooling from 300 K at 1 K min^{-1}, $\chi_M T$ was found to decrease with time to reach a minimum value; thereafter, the sample was cooled from 85 to 5 K at a sweep rate of 1 K min^{-1} (▽).

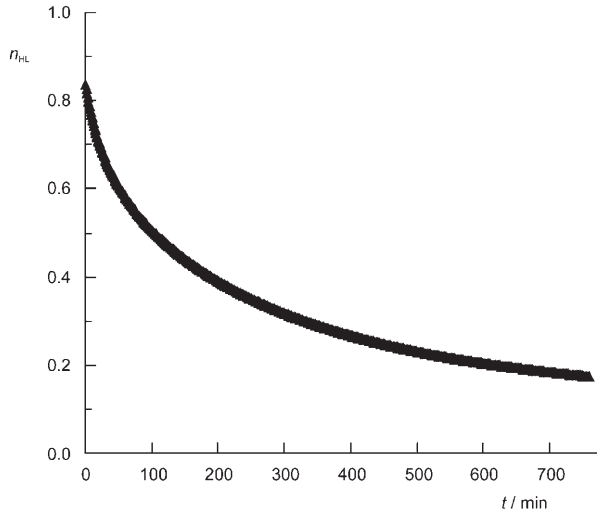

Figure 9. Time dependence of the normalized HS fraction (n_{HS}) at 85 K for $[Fe^{II}H_3L^{Me}]Cl{\cdot}AsF_6$ (**2**). The sample was maintained at 85 K after cooling from 300 K to 85 K at a sweep rate of 1 K min^{-1}.

state. As the temperature is raised, $\chi_M T$ increases to reach a plateau value of around 1.7 cm^3 K mol^{-1}, as expected for one half of the normal HS Fe^{II} complex. The decrease from the half-HS value in the lower temperature region can be ascribed to the zero-field splitting effect of the HS ($S = 2$) state. This result indicates that half of the HS Fe^{II} sites are frozen-in. Upon further increasing the temperature, $\chi_M T$ rapidly decreases to nearly zero at around 80 K, then rapidly increases beyond 90 K to reach the plateau value of 1.7 cm^3 K mol^{-1} in the temperature region 90–120 K, and finally steeply increases from 140 K to reach a plateau value of 3.5 cm^3 K mol^{-1}. This complicated magnetic behavior can be rationalized in terms of a two-step SC of the type HS ⇄ (HS + LS)/2 ⇄ LS exhibiting a thermal relaxation process, as evidenced by the measurements described below.

On lowering the temperature from 300 to 5 K at a rate of 1 K min^{-1} to acquire a second set of measurements, the $\chi_M T$ value of about 3.5 cm^3 K mol^{-1} is constant in the region 300–150 K, but then sharply decreases at around 130 K from about 3.5 cm^3 K mol^{-1} to a plateau value of 1.7 cm^3 K mol^{-1} (ca. half of the HS value), and thereafter shows a moderate decrease to 1.1 cm^3 K mol^{-1}. The inflection points for these first and second SC transitions are estimated to be at 122 and 82 K, respectively. The magnetic behavior thus shows a two-step spin transition, but the second SC in the lower temperature region is not perfect at the cooling rate of 1 K min^{-1} employed. To investigate this unusual SC behavior more closely, further magnetic measurements were carried out. After cooling the sample from 300 K at a rate of 1 K min^{-1}, the sample temperature was maintained at 85 K and the time dependence of the $\chi_M T$ value was measured. As shown in Figure 9, the $\chi_M T$ value at 85 K was seen to gradually decrease from 1.49 cm^3 K mol^{-1} at $t = 0$ min to 0.24 cm^3 K mol^{-1} at $t = 750$ min, demonstrating the existence of a thermal relaxation process. The decay curve shows a deviation from a simple exponential equation ($n_{HS} = \exp(-k_{HL}t)$).

Representative Mössbauer spectra recorded in the course of warming after a rapid cooling to 4.2 K and in the course of slow cooling from room temperature are shown in Figure 10a and b, respectively. In the heating mode, the spectrum at 4.2 K consists of two doublets attributable to the HS Fe^{II} ($\delta = 1.11$ mm s^{-1} and $\Delta E_Q = 2.16$ mm s^{-1}) and LS Fe^{II} ($\delta = 0.47$ mm s^{-1} and $\Delta E_Q = 0.23$ mm s^{-1}), with relative areas of 0.48 and 0.52. The spectrum recorded at 4.2 K after the rapid cooling indicates that about one half of the Fe^{II} sites are in the HS Fe^{II} state, thus corroborating the magnetic sus-

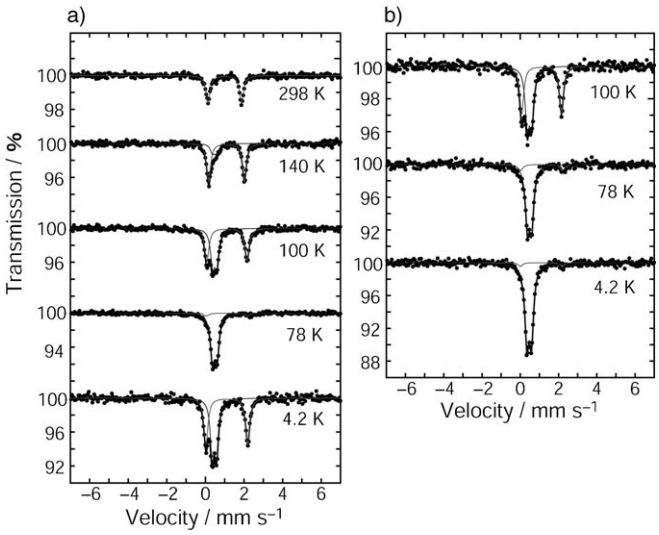

Figure 10. a) Selected ^{57}Fe Mössbauer spectra of $[Fe^{II}H_3L^{Me}]Cl{\cdot}AsF_6$ (**2**) recorded at 4.2, 50, 60, 78, 100, 120, 140, 170, 200, and 298 K during warming of the sample after rapid cooling from room temperature to 4.2 K. b) Selected ^{57}Fe Mössbauer spectra recorded at 4.2, 78, and 100 K during cooling.

ceptibility result. On increasing the temperature, the relative intensity of the doublet due to the HS Fe^{II} species abruptly decreases at around 60 K to reach 8% at 78 K and then sharply increases to 100% above 170 K, in the course of which an intermediate HS + LS state is clearly observed in the region 100–120 K. Above 170 K, the spectrum consists of a doublet attributable to the HS Fe^{II} species. On slowly cooling the sample from 298 K, the relative intensity of the doublet due to the HS Fe^{II} species decreases, while the doublet due to the LS Fe^{II} appears and intensifies. Although the time dependence of the thermal relaxation process was observed through the aforementioned magnetic susceptibility measurements at 85 K, it was not possible to observe this time dependence through the Mössbauer spectra at 78 K, probably due to the longer measurement time. A deconvolution analysis of the spectra was performed in order to determine the HS versus total Fe^{II} molar fraction, n_{HS}. The Mössbauer parameters are listed in Table 4, and plots of the variation of n_{HS} with temperature derived from the Mössbauer spectra are shown in Figure 11, together with the variation of n_{HS} derived from the magnetic susceptibility measurements. The plots are nearly the same for the warming and cooling modes. The Mössbauer and magnetic susceptibility results are consistent.

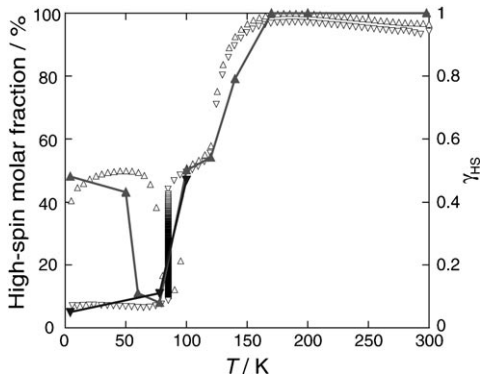

Figure 11. Molar fraction of HS versus total Fe^{II}, n_{HS}, for $[Fe^{II}H_3L^{Me}]Cl{\cdot}AsF_6$ (**2**) in the warming (▲) and cooling modes (▼) obtained by deconvolution analysis of the Mössbauer spectra, together with n_{HS} obtained from the magnetic susceptibility measurements. n_{HS} was calculated by using the equation $(\chi_M T)_{obs} = n_{HS}(\chi_M T)_{HS} + (1 - n_{HS})(\chi_M T)_{LS}$, with $(\chi_M T)_{HS} = 3.5\ cm^3 K mol^{-1}$ and $(\chi_M T)_{LS} = 0.0\ cm^3 K mol^{-1}$ as the limiting values.

Table 4. Mössbauer parameters for $[Fe^{II}H_3L^{Me}]Cl{\cdot}AsF_6$ (**2**).

A. On heating after rapid cooling to 4.2 K				
T [K]	δ[a] [mm s^{-1}]	ΔE_Q [mm s^{-1}]	Γ[b] [mm s^{-1}]	Relative area [%]
298	1.00	1.74	0.25	100
200	1.05	1.80	0.26	100
170	1.09	1.82	0.25	100
140	1.09	1.85	0.24	79
	0.48	0.21	0.28	21
120	1.10	1.99	0.25	54
	0.47	0.22	0.24	49
100	1.12	2.08	0.26	50
	0.48	0.22	0.25	50
78	1.11	2.14	0.30	8
	0.48	0.23	0.25	92
60	1.10	2.18	0.25	11
	0.46	0.23	0.28	89
50	1.13	2.18	0.25	43
	0.48	0.22	0.26	57
4.2	1.11	2.16	0.25	48
	0.47	0.23	0.23	52
B. On slow cooling from room temperature				
T [K]	δ[a] [mm s^{-1}]	ΔE_Q [mm s^{-1}]	Γ[b] [mm s^{-1}]	Relative area [%]
100	1.12	2.08	0.26	47
	0.48	0.22	0.25	53
78	1.11	2.17	0.30	11
	0.49	0.22	0.25	89
4.2	1.10	2.19	0.24	5
	0.47	0.24	0.27	95

[a] Isomer shift data are reported with respect to iron foil. [b] Full width at half-height.

To investigate the structures in the HS, (HS + LS)/2, and LS states, crystal structures were determined by single-crystal X-ray diffraction analysis at 180, 110, and 90 K. The sample was cooled to 90 K, taking into consideration the thermal relaxation observed in the magnetic measurements. Apart from the anions, the same atom-numbering scheme applies throughout. Table 5 shows selected bond lengths and hydrogen-bond lengths. The space group $P2_1/n$ adopted at 180 K becomes $P2_1$ at 110 K and then becomes $P2_1/n$ once more at 90 K. In the HS and LS states, the complex consists of one molecular unit (Figure 4) and assumes a similar 2D extended structure (Figure 6), while in the (HS + LS)/2 state it consists of two molecules and assumes a striped, layered structure (Figure 7). Although the number of unique molecules changes from one at 180 K to two at 110 K and back to one at 90 K, the crystal structures at the three temperatures are essentially the same except for the Fe^{II} environments. Thus, a 2D layered structure is formed, constructed by three imidazole NH···Cl^- hydrogen bonds around a Cl^- ion, a common network structural motif in the series $[Fe^{II}H_3L^{Me}]Cl{\cdot}X$, where the PF_6^- ion of **1** is replaced by the AsF_6^- ion in the present complex.

The $[Fe^{II}H_3L^{Me}]^{2+}$ ion is a chiral species with either a Δ (clockwise) or Λ (anticlockwise) configuration due to the screw coordination arrangement of the achiral tripod ligand around the Fe^{II} ion. At 180 and 90 K, there is only one unique molecule in the unit cell, in which the Δ and Λ enantiomers are related by a symmetry operation to give a racemic crystal. At 110 K, the chiral space group $P2_1$ is adopted, with either a combination of Δ-HS-Fe^{II} and Λ-LS-Fe^{II} or a combination of Λ-HS-Fe^{II} and Δ-LS-Fe^{II} being present in the crystal. As shown in Figure 5, the Δ (HS Fe1) and Λ (LS Fe2) enantiomers within a layer are connected by hydrogen bonds so as to form an alternating 2D array. The spin conversion from the HS (180 K) to the LS (90 K) state through the HS + LS (110 K) state can be rationalized in terms of a stable HS + LS state, as provided by the striped layer structure with different chiralities.

At 180 K, the Fe–N bond lengths (2.169(4)–2.211(4) Å) are typical of what one would expect for a high-spin Fe^{II}

Table 5. Relevant coordination bond lengths [Å], angles [°], and hydrogen-bond lengths [Å] for $[Fe^{II}H_3L^{Me}]Cl{\cdot}AsF_6$ (**2**) at 180, 110, and 90 K.

	180 K		110 K		90 K
Fe1–N2	2.177(3)		2.175(5)		1.978(9)
Fe1–N3	2.195(4)		2.207(5)		1.972(9)
Fe1–N5	2.182(4)		2.174(4)		1.945(9)
Fe1–N6	2.211(4)		2.192(5)		1.96(1)
Fe1–N8	2.169(4)		2.159(5)		1.97(1)
Fe1–N9	2.205(3)		2.211(5)		1.990(9)
Fe2–N12			1.979(5)		
Fe2–N13			2.013(5)		
Fe2–N15			1.987(5)		
Fe2–N16			1.991(5)		
Fe2–N18			1.996(5)		
Fe2–N19			1.999(4)		
hydrogen bonds					
	180 K		110 K		90 K
Cl1···N4[a]	3.086(4)	Cl1···N(14)[a]	3.105(5)	Cl1···N4[a]	3.12(1)
Cl1···N7[b]	3.051(4)	Cl1···N7[b]	3.062(5)	Cl1···N7[b]	3.02(1)
Cl1···N10	3.109(4)	Cl1···N10	3.105(5)	Cl1···N10	3.146(9)
		Cl2···N4[a]	3.072(3)		
		Cl2···N17[b]	3.052(3)		
		Cl2···N20	3.132(3)		

Symmetry operations: [a] $-x, -y, 1-z$; [b] $-x, {}^1/_2+y, {}^3/_2-z$.

complex with six similar N donor atoms. At 110 K, the crystallographically unique unit consists of two independent Fe^{II} sites, Fe1 and Fe2, where the Fe1–N bond lengths (2.159(5)–2.211(5) Å) and the Fe2–N bond lengths (1.979(5)–2.013(5) Å) are typical for a HS and LS Fe^{II} complex, respectively. The difference between the average Fe–N bond lengths at Fe1 and Fe2 is 0.192 Å, which is comparable to the HS-LS difference of 0.17 Å reported for Fe^{II} SC complexes with the same N_6 donor set, such as $[Fe^{II}H_3L^{Me}]$-$[Fe^{II}L^{Me}]PF_6$.[6c] The N-Fe-N bond angles also indicate that Fe1 assumes the HS state and that Fe2 assumes the LS state, since that at Fe2 is closer to the value for a regular octahedron than that at Fe1 (for example, N2-Fe-N3 77.1(2)°; N12-Fe2-N13 81.4(2)° at 110 K). At 90 K, the Fe–N bond lengths (1.945(9)–1.990(9) Å) are typical of what one would expect for a LS Fe^{II} complex. The average Fe–N bond length decreases by 0.221 Å from 2.190 Å at 180 K to 1.969 Å at 90 K. The N-Fe-N bond angles shift towards the value for a regular octahedron at 90 K (for example, N2-Fe-N3 76.4(1)° at 180 K, 81.2(4)° at 90 K).

SC properties and structure of $[Fe^{II}H_3L^{Me}]Cl{\cdot}SbF_6$ (3): Figure 12 shows $\chi_M T$ versus T plots in the cooling and warming modes for **3**, which displays a gradual one-step SC of the type HS ⇄ LS. A small difference between the warming and cooling modes is observed in the lower temperature region, indicative of a small frozen-in effect. On increasing the temperature from 5 K, the initial $\chi_M T$ value of 0.2 $cm^3 K mol^{-1}$, which is slightly higher than that of LS Fe^{II} ($S = 0$), remains essentially constant in the temperature range 5–80 K. The $\chi_M T$ value then decreases to nearly zero at around 90 K, but increases once more at around 120 K to reach the HS value. On lowering the temperature from 300 K to obtain a second set of measurements, $\chi_M T$ decreases from about 3.4 $cm^3 K mol^{-1}$ at 300 K to nearly zero at 5 K, showing a gradual one-step SC between the HS ($S = 2$) and LS ($S = 0$) states at $T_{1/2} = 117$ K.

Representative Mössbauer spectra recorded upon heating after rapid cooling to 4.2 K and upon slow cooling from room temperature are shown in Figure 13. In the range 4.2–78 K, the spectrum consists of a main doublet attributable to LS Fe^{II} (at 4.2 K; $\delta = 0.47$ $mm s^{-1}$, $\Delta E_Q = 0.24$ $mm s^{-1}$) and a small doublet attributable to HS Fe^{II} (at 4.2 K; $\delta = 1.11$ $mm s^{-1}$, $\Delta E_Q = 2.20$ $mm s^{-1}$). Upon increasing the sample temperature from 4.2 K, the relative intensity of the doublet due to the LS Fe^{II} species decreases, while the doublet due to the HS Fe^{II} species intensifies. A deconvolution analysis of the spectra was performed to determine the HS versus total Fe^{II} molar fraction, n_{HS}. The Mössbauer parameters are listed in Table 6. Plots of the variation of n_{HS} with temperature derived from the Mössbauer spectra and from the magnetic susceptibility measurements are shown in Figure 14. The plots are nearly the same for the warming and cooling modes. The Mössbauer and magnetic susceptibility results are almost consistent. The small frozen-in effect detected in the magnetic susceptibility measurements was not evident from the Mössbauer spectra.

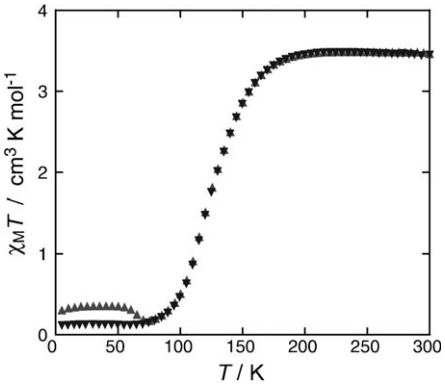

Figure 12. Magnetic behavior of $[Fe^{II}H_3L^{Me}]Cl{\cdot}SbF_6$ (**3**) in the form of $\chi_M T$ versus T plots in the warming and cooling modes. The sample was quickly cooled from 300 K to 5 K and $\chi_M T$ values were first measured in the course of warming from 5 to 300 K at a sweep rate of 1 $K min^{-1}$ (▲). Values were then measured in the course of cooling from 300 to 5 K at a sweep rate of 1 $K min^{-1}$ (▼).

Since the magnetic susceptibility and Mössbauer spectral measurements demonstrate that the complex assumes the

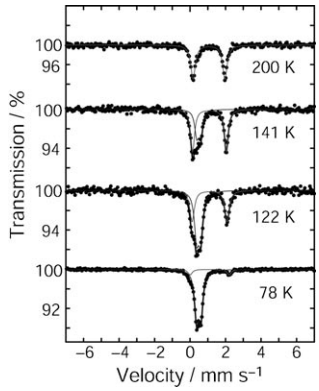

Figure 13. Selected ^{57}Fe Mössbauer spectra of $[Fe^{II}H_3L^{Me}]Cl{\cdot}SbF_6$ (**3**) recorded at 78, 122, 141, and 200 K upon warming the sample from 4.2 K.

Table 6. Mössbauer parameters for $[Fe^{II}H_3L^{Me}]Cl{\cdot}SbF_6$ (**3**).

A. On heating after rapid cooling to 4.2 K				
T [K]	δ[a] [mm s^{-1}]	ΔE_Q [mm s^{-1}]	Γ[b] [mm s^{-1}]	Relative area [%]
298	1.00	1.69	0.27	100
200	1.06	1.80	0.29	100
180	1.07	1.83	0.27	95
	0.46	0.21	0.24	5
160	1.07	1.86	0.28	86
	0.48	0.21	0.24	14
141	1.09	1.90	0.26	63
	0.49	0.22	0.26	37
122	1.10	1.97	0.30	43
	0.48	0.22	0.28	57
100	1.18	2.00	0.29	24
	0.48	0.22	0.26	76
78	1.10	2.21	0.29	12
	0.49	0.24	0.26	88
4.2	1.13	2.20	0.28	10
	0.48	0.24	0.26	90
B. On slow cooling from room temperature				
T [K]	δ[a] [mm s^{-1}]	ΔE_Q [mm s^{-1}]	Γ[b] [mm s^{-1}]	Relative area [%]
78	1.12	2.18	0.30	11
	0.48	0.23	0.26	89
4.2	1.11	2.20	0.28	8
	0.47	0.24	0.26	92

[a] Isomer shift data are reported with respect to iron foil. [b] Full width at half-height.

HS and LS states at 180 and 90 K, respectively, it was subjected to single-crystal X-ray diffraction analysis at these two temperatures. In the HS and LS states, the complex consists of a single crystallographically unique molecule (Figure 4) and assumes a similar 2D extended structure (Figure 6); as before, except for the anions, the same atom numbering scheme applies. Table 7 lists selected bond lengths and angles, together with the hydrogen-bond lengths. The structure consists of the $[Fe^{II}H_3L^{Me}]^{2+}$ ion and the Cl^- and SbF_6^- ions and assumes a 2D layered structure, again constructed by three imidazole NH···Cl^- hydrogen bonds, the common network structural motif in the $[Fe^{II}H_3L^{Me}]Cl{\cdot}X$ series.

The Fe^{II} ion assumes an octahedral coordination environment made up by the six N donor atoms, and the Fe–N

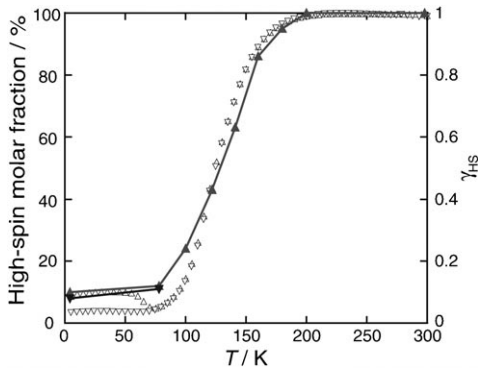

Figure 14. Molar fraction of HS versus total Fe^{II}, n_{HS}, for $[Fe^{II}H_3L^{Me}]Cl{\cdot}SbF_6$ (**3**) in the warming (▲) and cooling modes (▼) obtained by deconvolution analysis of the Mössbauer spectra, together with n_{HS} obtained from the magnetic susceptibility measurements. n_{HS} was calculated by using the equation $(\chi_M T)_{obs} = n_{HS}(\chi_M T)_{HS} + (1 - n_{HS})(\chi_M T)_{LS}$, with $(\chi_M T)_{HS} = 3.5\ cm^3 K mol^{-1}$ and $(\chi_M T)_{LS} = 0.0\ cm^3 K mol^{-1}$ as limiting values.

Table 7. Relevant coordination bond lengths [Å], angles [°], and hydrogen-bond lengths [Å] for $[Fe^{II}H_3L^{Me}]Cl{\cdot}SbF_6$ (**3**) at 180 and 90 K.

	180 K		90 K
Fe1–N2	2.179(2)		1.997(2)
Fe1–N3	2.204(2)		2.013(2)
Fe1–N5	2.179(2)		2.008(2)
Fe1–N6	2.197(2)		2.007(2)
Fe1–N8	2.170(2)		2.002(2)
Fe1–N9	2.206(2)		2.015(2)
hydrogen bonds			
	180 K		90 K
Cl1···N4[a]	3.081(2)	Cl1···N4[a]	3.099(2)
Cl1···N7[b]	3.052(2)	Cl1···N(7)[b]	3.056(2)
Cl1···N(10)	3.100(2)	Cl1···N(10)	3.121(2)

Symmetry operations: [a] $-x, -y, 1 - z$; [b] $-x, {}^1/_2 + y, {}^3/_2 - z$

bond lengths are 2.170(2)–2.206(2) Å at 180 K and 1.997(2)–2.015(2) Å at 90 K. The average Fe–N bond length decreases by 0.182 Å from 2.189 Å at 180 K to 2.007 Å at 90 K. The N-Fe-N bond angles shift towards the value for a regular octahedron at 90 K (for example, N2-Fe-N3 = 76.66(8)° at 180 K, 81.29(8)° at 90 K).

SC properties and structure of $[Fe^{II}H_3L^{Me}]Cl{\cdot}CF_3SO_3$ (4): Figure 15 shows $\chi_M T$ versus T plots, which are indicative of a steep one-step SC of the type HS ⇄ LS and a perfect frozen-in effect. In the first set of measurements, the $\chi_M T$ value of 2.7 $cm^3 K mol^{-1}$ at 4.2 K after rapid cooling is lower than that expected for the HS ($S = 2$) Fe^{II} state, but the value increases to reach a plateau value of about 3.5 $cm^3 K mol^{-1}$, as would be expected. Such a decrease from the HS value in the low-temperature region is frequently observed for HS Fe^{II} complexes, and is ascribed to zero-field splitting. On increasing the temperature further, $\chi_M T$ rapidly decreases at around 80 K and then rapidly increases to reach the HS value of 3.5 $cm^3 K mol^{-1}$, reflecting the thermal relaxation from the HS to the LS state at around 75 K and

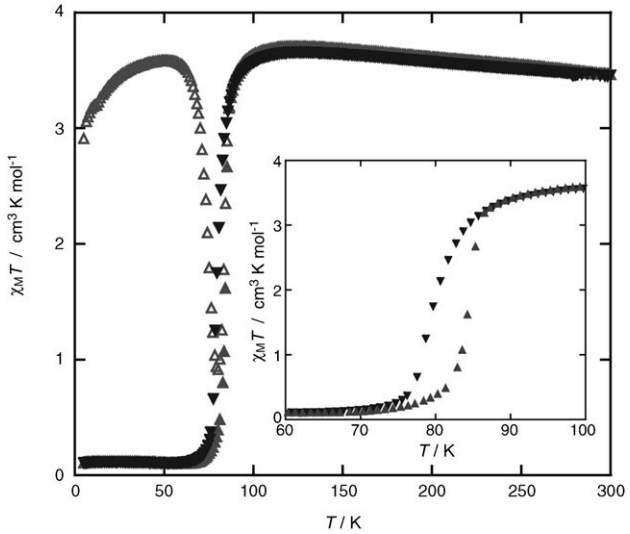

Figure 15. Magnetic behavior of $[Fe^{II}H_3L^{Me}]Cl{\cdot}CF_3SO_3$ (**4**) in the form of $\chi_M T$ versus T plots in the warming and cooling modes. The sample was quickly cooled from 300 to 5 K and $\chi_M T$ values were first measured in the course of warming from 5 to 300 K at a sweep rate of 1 K min^{-1} (▲). Values were then measured in the course of cooling from 300 to 5 K at a sweep rate of 1 K min^{-1} (▼). The inset figure reveals hysteresis.

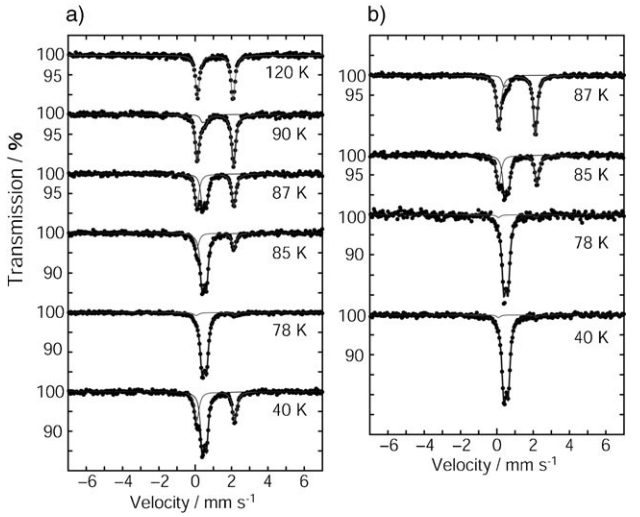

Figure 16. a) Selected ^{57}Fe Mössbauer spectra of $[Fe^{II}H_3L^{Me}]Cl{\cdot}CF_3SO_3$ (**4**) recorded at 40, 78, 85, 87, 90, and 120 K upon warming the sample after rapid cooling to 4.2 K. b) Selected ^{57}Fe Mössbauer spectra recorded at 87, 85, 78, and 40 K upon gradual cooling from 300 K.

the spin transition from the LS to the HS state at around 80 K.

On lowering the temperature from 300 K to 5 K at a rate of 1 K min^{-1}, the $\chi_M T$ value of about 3.7 cm^3 K mol^{-1} is constant in the region 300–100 K, but then steeply decreases at around 80 K from about 3.5 cm^3 K mol^{-1} to nearly zero. As shown in Figure 15 (inset), the third (warming mode) and fourth (cooling mode) sets of measurements reveal hysteresis, and the evaluated $T_{1/2\uparrow}$ and $T_{1/2\downarrow}$ values are 84 and 80 K, respectively.

Representative Mössbauer spectra are shown in Figure 16a and b. On increasing the temperature of the sample after rapid cooling to 4.2 K, spectra were recorded at 4.2, 40, 78, 85, 87, 90, 120, and 298 K. At 4.2 K, the spectrum consists of two doublets attributable to HS Fe^{II} (δ = 1.13 mm s^{-1} and ΔE_Q = 2.09 mm s^{-1}) and LS Fe^{II} (δ = 0.5 mm s^{-1}, ΔE_Q = 0.23 mm s^{-1}) in an intensity ratio of 48:52. This result indicates that one half of the HS Fe^{II} is frozen, which is at variance with the magnetic susceptibility result. This inconsistency may be due to the difference in the cooling times, since the sample used to obtain the Mössbauer spectrum was cooled from 298 to 4.2 K over 3 min, whereas the sample that provided the magnetic susceptibility data was cooled within a few seconds. At 78 K, the doublet due to the HS Fe^{II} species has almost disappeared and the doublet due to the LS species is the main peak, indicating that the frozen HS Fe^{II} species converts to the LS state due to thermal relaxation. On further increasing the temperature from 78 K, the relative intensity of the doublet due to the LS state decreases, while that of the doublet due to the HS state increases, showing a steep one-step SC behavior. Above 120 K, only the doublet due to the HS species is observed. During slow cooling of the sample from 298 K to 4.2 K, Mössbauer spectra were recorded at 90, 87, 85, 78, 40, and 4.2 K. At 90 K, the spectrum consists of a main doublet attributable to HS Fe^{II} (δ = 1.12 mm s^{-1} and ΔE_Q = 2.01 mm s^{-1}) and a small doublet attributable to LS Fe^{II} (δ = 0.49 mm s^{-1} and ΔE_Q = 0.22 mm s^{-1}). On lowering the temperature, the relative intensity of the doublet due to the HS Fe^{II} species decreases, while that of the doublet due to the LS Fe^{II} increases.

A deconvolution analysis of the spectra was performed to determine the HS versus total Fe^{II} molar fraction, n_{HS}. The Mössbauer parameters are listed in Table 8, and plots of the variation of n_{HS} with temperature are shown in Figure 17. As is clearly apparent from Figure 17 and Table 8, the Mössbauer and magnetic susceptibility results are not consistent in the low-temperature region and hysteresis is observed in the Mössbauer measurements.

The crystal structure was determined by single-crystal X-ray diffraction analysis at 296 K. Table 9 shows selected bond lengths and hydrogen-bond lengths. The complex assumes a 2D layered structure constructed by three imidazole NH···Cl$^-$ hydrogen bonds (see Table 9), the common network structural motif for $[Fe^{II}H_3L^{Me}]Cl{\cdot}X$. At 296 K, the Fe–N bond lengths are distributed in the range 2.165(2)–2.236(2) Å and the average value is 2.202 Å, which is typical of what one would expect for a HS Fe^{II} complex with coordination by six similar N atoms.

Concluding Remarks

As described above, a variety of SC behaviors, namely 1) a one-step SC of the type HS ⇄ (HS + LS)/2, 2) a two-step SC of the type HS ⇄ (HS + LS)/2 ⇄ LS, 3) a gradual one-

Table 8. Mössbauer parameters for $[Fe^{II}H_3L^{Me}]Cl{\cdot}CF_3SO_3$ (**4**).

A. On heating after rapid cooling to 4.2 K				
T [K]	δ[a] [mm s^{-1}]	ΔE_Q [mm s^{-1}]	Γ[b] [mm s^{-1}]	Relative area [%]
298	1.00	1.76	0.24	100
120	1.05	1.80	0.26	100
90	1.11	2.00	0.26	89
	0.48	0.20	0.25	11
87	1.11	2.03	0.26	58
	0.51	0.23	0.23	42
85	1.11	2.03	0.26	27
	0.50	0.23	0.25	73
78	1.13	2.08	0.29	6
	0.50	0.24	0.27	94
40	1.13	2.08	0.25	42
	0.50	0.23	0.24	58
4.2	1.13	2.09	0.27	48
	0.50	0.23	0.24	52
B. On slow cooling from room temperature				
T [K]	δ[a] [mm s^{-1}]	ΔE_Q [mm s^{-1}]	Γ[b] [mm s^{-1}]	Relative area [%]
90	1.12	2.01	0.25	90
	0.49	0.22	0.25	10
87	1.12	2.02	0.26	85
	0.50	0.23	0.23	15
85	1.14	2.08	0.28	57
	0.52	0.23	0.24	43
78	1.13	2.07	0.25	4
	0.50	0.23	0.25	96
40	1.13	2.08	0.25	3
	0.50	0.23	0.27	97
4.2	1.12	2.12	0.25	6
	0.50	0.24	0.27	94

[a] Isomer shift data are reported with respect to iron foil. [b] Full width at half-height.

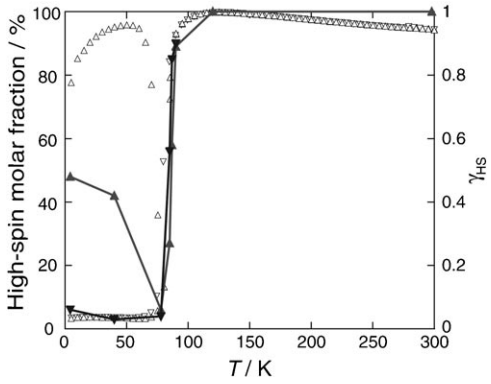

Figure 17. Molar fraction of HS versus total Fe^{II}, n_{HS}, for $[Fe^{II}H_3L^{Me}]Cl{\cdot}CF_3SO_3$ (**4**) in the warming (▲) and cooling modes (▼) obtained by deconvolution analysis of the Mössbauer spectra, together with n_{HS} obtained from the magnetic susceptibility measurements. n_{HS} was calculated by using the equation $(\chi_M T)_{obs} = n_{HS}(\chi_M T)_{HS} + (1 - n_{HS})(\chi_M T)_{LS}$, with $(\chi_M T)_{HS} = 3.5\,cm^3\,K\,mol^{-1}$ and $(\chi_M T)_{LS} = 0.0\,cm^3\,K\,mol^{-1}$ as the limiting values.

step SC of the type HS ⇄ LS, and 4) a steep one-step SC of the type HS ⇄ LS with hysteresis, has been observed in a series of complexes with the general formula $[Fe^{II}H_3L^{Me}]Cl{\cdot}X$ ($X^- = PF_6^-$, AsF_6^-, SbF_6^-, $CF_3SO_3^-$) (**1**–**4**). These complexes not only crystallized in the same monoclinic crystal system with similar cell dimensions, but also assumed the same space groups, that is, $P2_1/n$ in the HS state, $P2_1$ in the HS + LS state, and $P2_1/n$ in the LS state. The general crystal structure consists of a 2D extended network constructed by NH···Cl^- hydrogen bonds between Cl^- and the imidazole NH groups of three neighboring $[Fe^{II}H_3L^{Me}]^{2+}$ cations, while the anion X exists as an isolated counter anion and occupies the space between the 2D sheets. It can easily be envisaged how the size of the counter anion might affect the 2D network structure leading to modifications of the SC behavior, since the present 2D network structure constructed by the hydrogen bonds is quite flexible and a counter anion residing in the space between the 2D sheets may well lead to some distortion of the network. The molecular volumes, V, of the counter anions have been evaluated by quantum-chemical calculations[10] as follows: 53.4 Å^3 for BF_4^-, 54.4 Å^3 for ClO_4^-, 73.0 Å^3 for PF_6^-, 78.5 Å^3 for AsF_6^-, 88.7 Å^3 for SbF_6^-, 86.9 Å^3 for $CF_3SO_3^-$, and 94.4 Å^3 for I_3^-. These estimated relative sizes and the shapes of the counter anions can be correlated with the crystal structures and SC behaviors. The salts with the smaller counter anions BF_4^- and ClO_4^- have the chemical formula $[Fe^{II}H_3L^{Me}]X_2$. These anions are too small to occupy the space between the 2D sheets, and so these complexes cannot assume the formula $[Fe^{II}H_3L^{Me}]Cl{\cdot}X$ with the 2D structure. The salts with the anions of intermediate size, PF_6^- and AsF_6^-, assume the chemical formula $[Fe^{II}H_3L^{Me}]Cl{\cdot}X$ and exhibit a two-step SC behavior involving the HS + LS state. The salts with the large-sized anions, SbF_6^-, $CF_3SO_3^-$, and I_3^-,[8] assume the chemical formula $[Fe^{II}H_3L^{Me}]Cl{\cdot}X$ and exhibit one-step SC behavior, where the SbF_6^- salt shows a gradual SC behavior and the latter two salts show a steep SC behavior. From this, it is apparent that the shape of the counter anion can also affect the SC behavior, since despite having almost the same molecular volume, the SbF_6^- and $CF_3SO_3^-$ ions assume a sphere and a dumbbell shape, respectively, while the much larger anion I_3^- assumes a cylindrical shape.

Table 9. Relevant coordination bond lengths [Å], angles [°], and hydrogen-bond lengths [Å] for $[Fe^{II}H_3L^{Me}]Cl{\cdot}CF_3SO_3$ (**4**) at 296 K.

	296 K
Fe1–N2	2.179(2)
Fe1–N3	2.233(2)
Fe1–N5	2.176(2)
Fe1–N6	2.225(2)
Fe1–N8	2.165(2)
Fe1–N9	2.236(2)
hydrogen bonds	
	296 K
Cl1···N4[a]	3.139(2)
Cl1···N7[b]	3.112(2)
Cl1···N10	3.144(2)

Symmetry operations: [a] $-x, -y, 1 - z$; [b] $-x, {}^1/_2 + y, {}^3/_2 - z$.

The network of these 2D sheets consists of fused binuclear and tetranuclear cyclic structures made up of two and four $[Fe^{II}H_3L^{Me}]^{2+}$ units, respectively, connected by Cl^--mediated hydrogen bonds; see Figure 4b and Figure 5a. As a consequence of this network structure, each $[Fe^{II}H_3L^{Me}]^{2+}$ unit on one of the alternate rows of the Fe sites with the Δ

and Λ configuration that make up the 2D sheet forms a binuclear cyclic structure with a unit of opposite chirality on an adjacent row and two tetranuclear cyclic structures with one unit on the same row and two on the adjacent rows. Moreover, one of the counter anions shows significant contacts (ca. 0.2 Å shorter than the sum of the van der Waals radii) with methyl, imino, and imidazole hydrogen atoms on the units of the binuclear cyclic structure. Therefore, the entire 2D structure can be considered to be made up of loosely interacting dimers of $[Fe^{II}H_3L^{Me}]^{2+}$ units. This picture allows simulation of the SC behavior by the theoretical model developed by Real et al. for Fe^{II} binuclear compounds.[11] In this model, three possible states are allowed for the binuclear molecules, [LS-LS], [LS-HS], and [HS-HS], and it is assumed that the enthalpy of the [HS-LS] state does not exactly correspond to the average enthalpy of the [HS-HS] and [LS-LS] states. Writing $H_{HS\text{-}LS} = (H_{LS\text{-}LS} + H_{HS\text{-}HS})/2 + W$, where W is a small positive or negative intradimer interaction parameter, and assuming an excess Gibbs free energy due to intermolecular interactions and described by an interaction parameter γ, they showed that a two-step transition may be observed only if $W \leq 0$ and γ is sufficiently large. In other words, the two-step character of a transition arises from a synergy between an intramolecular interaction favoring the mixed-spin [HS-LS] state and intermolecular interactions favoring the formation of domains consisting of identical spin states. This approach can be used to explain the present SC behavior. According to the model of Real et al., it seems that the increase in the size of the counter anion in the series PF_6^-, AsF_6^-, SbF_6^-, $CF_3SO_3^-$, and I_3^-, while maintaining the same crystal structure leads to a decrease in both the stabilization of the intradimer interaction and the interdimer interactions. This is probably achieved through subtle intra- and interlayer modification or distortion of the 2D layer with increasing size of the counter anion.

It should be noted that the two-step transition for mononuclear Fe^{II} complexes has also been explained using the following approaches: 1) the compounds have a low-symmetry structure with nonequivalent crystallographic sites;[12] 2) the complexes have all equivalent lattice sites but strong nearest-neighbor interactions operating among them leads to the formation of superstructures and correlations, as in the first observed stepwise thermal spin transition of $[Fe^{II}(2\text{-pic})_3]Cl_2 \cdot EtOH$ (2-pic = 2-picolylamine);[13] 3) the spin transition in the compounds is coupled to a crystallographic phase transition.[14]

Thus, the present SC complexes constitute very useful model compounds for experimental and theoretical investigation of the exact microscopic origin of the multistep spin transition. It is hoped that further studies, including calorimetric measurements and investigation of the LIESST and thermal relaxation processes, as well as a theoretical approach, will provide the relevant information for a full understanding of the SC mechanism.

Experimental Section

General: All chemicals and solvents, obtained from Tokyo Kasei Co., Ltd., and Wako Pure Chemical Industries, Ltd., were of reagent grade and were used for the syntheses without further purification. All the synthetic procedures were carried out in air.

$[Fe^{II}H_3L^{Me}]Cl \cdot PF_6$ (1): Tris(2-aminoethyl)amine (0.731 g, 5 mmol) was added to a solution of 2-methyl-4-formylimidazole (2.58 g, 15 mmol) in acetonitrile (20 mL) and the mixture was stirred at 50 °C for 10 min. The solution of the tripod-like ligand (5 mmol) thus prepared was treated with a solution of $Fe^{II}Cl_2 \cdot 4H_2O$ (0.994 g, 5 mmol) in water (10 mL), followed by a solution of KPF_6 (1.84 g, 10 mmol) in acetonitrile (20 mL). The mixture was stirred overnight and then filtered. The filtrate was allowed to stand for several days, during which the precipitated orange crystals were collected by suction filtration and dried in vacuo to provide a 25% yield. Elemental analysis calcd (%) for $[Fe^{II}H_3L^{Me}]Cl \cdot PF_6$: C 38.29, H 4.59, N 21.26; found: C 38.06, H 4.39, N 21.86; IR (KBr): $\tilde{\nu}$ = 1641 ($\nu_{C=N}$), 844 (ν_{P-F} (PF_6^-)) cm^{-1}.

$[Fe^{II}H_3L^{Me}]Cl \cdot AsF_6$ (2), $[Fe^{II}H_3L^{Me}]Cl \cdot SbF_6$ (3), and $[Fe^{II}H_3L^{Me}]Cl \cdot CF_3SO_3$ (4): These complexes were prepared by way of a similar synthetic procedure, employing methanol as the reaction solvent. The synthesis of **2** is representative. A solution of the tripod-like ligand (5 mmol) in methanol (30 mL) was treated first with a solution of $Fe^{II}Cl_2 \cdot 4H_2O$ (0.994 g, 5 mmol) in methanol (10 mL) and then with a solution of $NaAsF_6$ (2.11 g, 10 mmol) in methanol (20 mL). The mixture was stirred for 1 h and then filtered. The filtrate was allowed to stand for several days, during which the precipitated orange crystals were collected by suction filtration and dried in vacuo. Well-grown dark-orange crystals were obtained in yields of 25% (**2**), 39% (**3**), and 34% (**4**). Elemental analysis calcd (%) for $[Fe^{II}H_3L^{Me}]Cl \cdot AsF_6$ (**2**): C 35.89, H 4.30, N 19.93; found: C 35.87, H 4.25, N 20.10; IR (KBr): $\tilde{\nu}$ = 1640 ($\nu_{C=N}$), 703 (ν_{As-F}-(AsF_6^-) cm^{-1}; elemental analysis calcd (%) for $[Fe^{II}H_3L^{Me}]Cl \cdot SbF_6$ (**3**): C 33.65, H 4.03, N 18.69; found C 33.72, H 4.02, N 18.78; IR (KBr): $\tilde{\nu}$ = 1640 ($\nu_{C=N}$), 661 (ν_{Sb-F}(SbF_6^-)) cm^{-1}; elemental analysis calcd. for $[Fe^{II}H_3L^{Me}]Cl \cdot CF_3SO_3$ (**4**): C 39.86, H 4.56, N 21.13; found C 39.54, H 4.58, N 20.99; IR (KBr): $\nu_{C=N}$ = 1640 cm^{-1}, ν_{C-F}($CF_3SO_3^-$) = 1268 cm^{-1}.

Physical measurements: C, H, and N elemental analyses were performed by Miss Kikue Nishiyama at the Center for Instrumental Analysis of Kumamoto University. Infrared spectra were recorded at room temperature using a Perkin-Elmer FT-IR PARAGON 1000 spectrometer with samples in KBr disks. Magnetic susceptibilities were measured in the 5–300 K temperature range, at a sweep rate of 1 K min^{-1}, under an applied magnetic field of 1 T, using an MPMS5 SQUID susceptometer (Quantum Design). The apparatus was calibrated with palladium metal. Corrections for diamagnetism were applied by using Pascal's constants.[15] Mössbauer spectra were recorded using a Wissel 1200 spectrometer and a proportional counter. $^{57}Co(Rh)$ moving in a constant acceleration mode was used as the radioactive source. Hyperfine parameters were obtained by a least-squares fitting of the Lorentzian peaks. Isomer shifts are reported relative to iron foil at 293 K. The sample temperature was controlled by means of a Heli-tran liquid-transfer refrigerator (Air Products and Chemicals, Inc.) to within an accuracy of ±0.5 K.

X-ray crystallography: X-ray diffraction data for **1, 2**, and **4** were collected by using a Rigaku RAXIS RAPID imaging plate diffractometer with graphite-monochromated $Mo_{K\alpha}$ radiation (λ = 0.71073 Å). The temperature of the crystal was maintained at the selected value by means of a Rigaku cooling device to within an accuracy of ±2 K. The data were corrected for Lorentz, polarization, and absorption effects. The structures were solved by direct methods and expanded using the Fourier technique.[16] Hydrogen atoms were fixed in calculated positions and refined by using a riding model. All calculations were performed by using the Crystal Structure crystallographic software package.[17]

Crystal structures of **3** were collected at 180 and 90 K by using an Oxford Diffraction Xcalibur diffractometer. The selected crystal was mounted on a diffractometer equipped with an Oxford Instruments Cryojet cooler device[18] and examined by using graphite-monochromated $Mo_{K\alpha}$ radiation (λ = 0.71073 Å). Gaussian absorption corrections were applied. The

structures were solved by direct methods using SHELXS-97[19] and refined against F^2 by full-matrix least-squares techniques using SHELXL-97[20] with anisotropic displacement parameters for all non-hydrogen atoms. The SbF_6^- anion appeared to be disordered. The occupancy factors were refined in the ratio 60:40 for the Sb atom and four F atoms, the two other F atoms being refined with an occupancy factor of 1.0. Hydrogen atoms were located on a difference Fourier map and introduced into the calculations as a riding model with isotropic thermal parameters 1.1 times higher than those of the atom to which they are bonded. Scattering factors were taken from reference [21]. Other atomic scattering factors and anomalous dispersion terms were taken from a standard compilation.[10] The crystal data collection and refinement parameters for **1, 2, 3**, and **4** are given in Table 1.

Theoretical calculations: Quantum chemical calculations were performed using the Spartan Package.[19] Geometry optimizations were performed on all of the considered counter anions using the PM3 semiempirical molecular orbital method and molecular volumes were then estimated at the same level of theory. The molecular volume obtained by this method represents an isodensity surface and was derived by considering an electron density of 0.002 a.u.

Acknowledgements

This work was supported by Grants in Aid of Science Research (nos. 16205010 and 17350028) from the Ministry of Education, Science, Sports, and Culture, Japan.

[1] a) For a general overview, see: P. Gütlich, H. A. Goodwin, Spin Crossover in Transition Metal Compounds 1 (Eds.: P. Gütlich, H. A. Goodwin), *Top. Curr. Chem.* **2004**, *233*; b) E. König, *Prog. Inorg. Chem.* **1987**, *35*, 527–623; c) E. König, *Struct. Bonding (Berlin)* **1991**, *76*, 51; d) H. A. Goodwin, *Coord. Chem. Rev.* **1976**, *18*, 293–325; e) P. Gütlich, A. Hauser, H. Spiering, *Angew. Chem.* **1994**, *106*, 2109–2141; *Angew. Chem. Int. Ed. Engl.* **1994**, *33*, 2024–2054.

[2] a) S. Decurtins, P. Gütlich, C. P. Kohler, H. Spiering, A. Hauser, *Chem. Phys. Lett.* **1984**, *105*, 1–4; b) P. Gütlich, Y. Garcia, T. Woike, *Coord. Chem. Rev.* **2001**, *219–221*, 839–879; c) A. Hauser, *J. Chem. Phys.* **1991**, *94*, 2741–2748.

[3] a) O. Kahn, J. C. Martinez, *Science* **1998**, *279*, 44–48; b) P. J. van Koningsbruggen, Y. Garcia, O. Kahn, L. Fournes, H. Kooijman, A. L. Spek, J. G. Haasnoot, J. Moscovici, K. Provost, A. Michalowicz, F. Renz, P. Gütlich, *Inorg. Chem.* **2000**, *39*, 1891–1900; c) J. A. Real, E. Andres, M. C. Muñoz, M. Julve, T. Granier, A. Bousseksou, F. Varret, *Science* **1995**, *268*, 265–267.

[4] a) Y. Garcia, O. Kahn, L. Rabardel, B. Chansou, L. Salmon, J.-P. Tuchagues, *Inorg. Chem.* **1999**, *38*, 4663–4670; b) E. Breuning, M. Ruben, J.-M. Lehn, F. Renz, Y. Garcia, V. Ksenofontov, P. Gütlich, E. Wegelius, K. Rissanen, *Angew. Chem.* **2000**, *112*, 2563–2566; *Angew. Chem. Int. Ed.* **2000**, *39*, 2504–2507; c) N. Moliner, C. Muñoz, S. Letard, X. Solans, N. Menendez, A. Goujon, F. Varret, J. A. Real, *Inorg. Chem.* **2000**, *39*, 5390–5393.

[5] a) S. Hayami, Z. Gu, M. Shiro, Y. Einaga, A. Fujishima, O. Sato, *J. Am. Chem. Soc.* **2000**, *122*, 7126–7127; b) S. Hayami, Z. Gu, H. Yoshiki, A. Fujishima, O. Sato, *J. Am. Chem. Soc.* **2001**, *123*, 11644–11650; c) R. Boca, M. Boca, L. Dihan, K. Falk, H. Fuess, W. Haase, R. Jarosciak, B. Papankova, F. Renz, M. Vrbova, R. Werner, *Inorg. Chem.* **2001**, *40*, 3025–3033.

[6] a) Y. Sunatsuki, Y. Ikuta, N. Matsumoto, H. Ohta, M. Kojima, S. Iijima, S. Hayami, Y. Maeda, S. Kaizaki, F. Dahan, J.-P. Tuchagues, *Angew. Chem.* **2003**, *115*, 1652–1656; *Angew. Chem. Int. Ed.* **2003**, *42*, 1614–1618; b) Y. Ikuta, M. Ooidemizu, Y. Yamahata, M. Yamada, S. Osa, N. Matsumoto, S. Iijima, Y. Sunatsuki, M. Kojima, F. Dahan, J.-P. Tuchagues, *Inorg. Chem.* **2003**, *42*, 7001–7017; c) M. Yamada, M. Ooidemizu, Y. Ikuta, S. Osa, N. Matsumoto, S. Iijima, M. Kojima, F. Dahan, J.-P. Tuchagues, *Inorg. Chem.* **2003**, *42*, 8406–8416; d) Y. Sunatsuki, H. Ohta, M. Kojima, Y. Ikuta, Y. Goto, N. Matsumoto, S. Iijima, H. Akashi, S. Kaizaki, F. Dahan, J.-P. Tuchagues, *Inorg. Chem.* **2004**, *43*, 4154–4171.

[7] a) I. Katsuki, Y. Motoda, Y. Sunatsuki, N. Matsumoto, T. Nakashima, M. Kojima, *J. Am. Chem. Soc.* **2002**, *124*, 629–640; b) M. Mimura, T. Matsuo, Y. Motoda, N. Matsumoto, T. Nakashima, M. Kojima, *Chem. Lett.* **1998**, 691–692; c) Y. Sunatsuki, Y. Motoda, N. Matsumoto, *Coord. Chem. Rev.* **2002**, *226*, 199–209; d) Y. Shii, Y. Motoda, T. Matsuo, F. Kai, T. Nakashima, J.-P. Tuchagues, N. Matsumoto, *Inorg. Chem.* **1999**, *38*, 3513–3522.

[8] M. Yamada, N. Matsumoto, M. Kojima, F. Dahan, J.-P. Tuchagues, S. Iijima, *Inorg. Chem.* **2005**, *44*, 6967–6974.

[9] K. Nakamoto, in *Infrared and Raman Spectra of Inorganic and Coordination Compounds*, 5th ed., Wiley, New York, **1997**, Part B, Chapter III, 14.

[10] Spartan, Version 4.0, Wavefunction, Inc., Irvine, California, **1999**.

[11] a) J. A. Real, H. Bolvin, A. Bousseksou, A. Dworkin, O. Kahn, F. Varret, J. Zarembowitch, *J. Am. Chem. Soc.* **1992**, *114*, 4650–4658; b) J. A. Real, A. B. Gaspar, M. C. Muñoz, P. Gütlich, V. Ksenofontov, H. Spiering, "Bipyrimidine-Bridged Dinuclear Iron(II) Spin-Crossover Compounds", in Spin Crossover in Transition Metal Compounds I (Eds.: P. Gütlich, H. A. Goodwin), *Top. Curr. Chem.* **2004**, *233*, 167–193.

[12] S. Decurtins, P. Gütlich, C. P. Kohler, H. Spiering, A. Hauser, *Chem. Phys. Lett.* **1984**, *105*, 1–4.

[13] R. Hinek, H. Spiering, D. Schollmeyer, P. Gütlich, A. Hauser, *Chem. Eur. J.* **1996**, *2*, 1127.

[14] D. Boinnard, A. Bousseksou, A. Dworkin, J.-M. Savariault, F. Varret, J.-P. Tuchagues, *Inorg. Chem.* **1994**, *33*, 271–281.

[15] O. Kahn, *Molecular Magnetism*, VCH, Weinheim, **1993**.

[16] P. T. Beurskens, G. Admiraal, G. Beurskens, W. P. Bosman, R. de Gelder, R. Israel, J. M. M. Smits, *The DIRDIF-99 program system*, Technical Report of the Crystallography Laboratory, University of Nijmegen, The Netherlands, **1999**.

[17] CrystalStructure 3.6.0, Crystal Structure Analysis Package, Rigaku and Rigaku/MSC (2000–2004), 9009 New Trails Dr., The Woodlands, TX 77381 USA.

[18] CRYSTALS Issue 11, D. J. Watkin, C. K. Prout, J. R. Carruthers, P. W. Betteridge, Chemical Crystallography Laboratory, Oxford, UK, CRYSALIS Version 170, Oxford Diffraction, **2002**.

[19] G. M. Sheldrick, SHELXS-97, Program for Crystal Structure Solution, University of Göttingen, Göttingen, Germany, **1990**.

[20] G. M. Sheldrick, SHELXL-97, Program for the refinement of crystal structures from diffraction data, University of Göttingen, Göttingen, Germany, **1997**.

[21] *International Tables for Crystallography, Vol. C*, Kluwer Academic Publishers, Dordrecht, The Netherlands, **1992**.

Received: August 10, 2005
Revised: December 26, 2005
Published online: March 31, 2006

